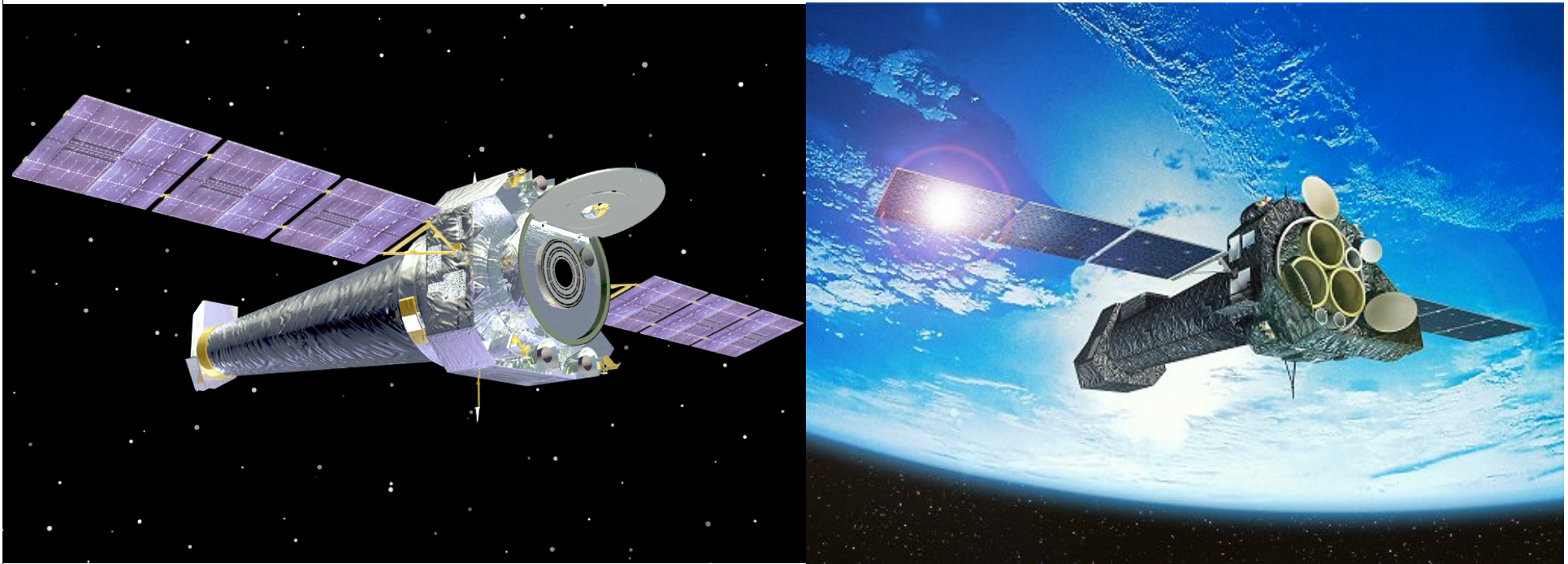


High-Resolution X-ray Spectra of magnetic CVs

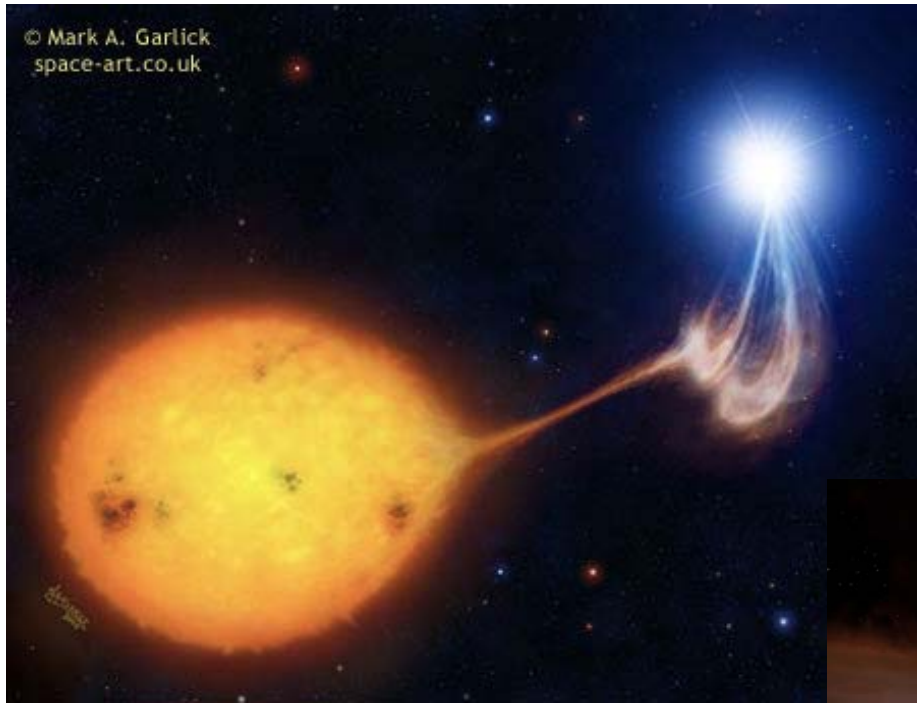


Vadim Burwitz (MPE)

MSSL, March 28, 2006



Magnetic cataclysmic variables (mCVs)



Polars

$$P_{\text{orb}} = P_{\text{spin}} \text{ (synchronous)}$$

No accretion disk

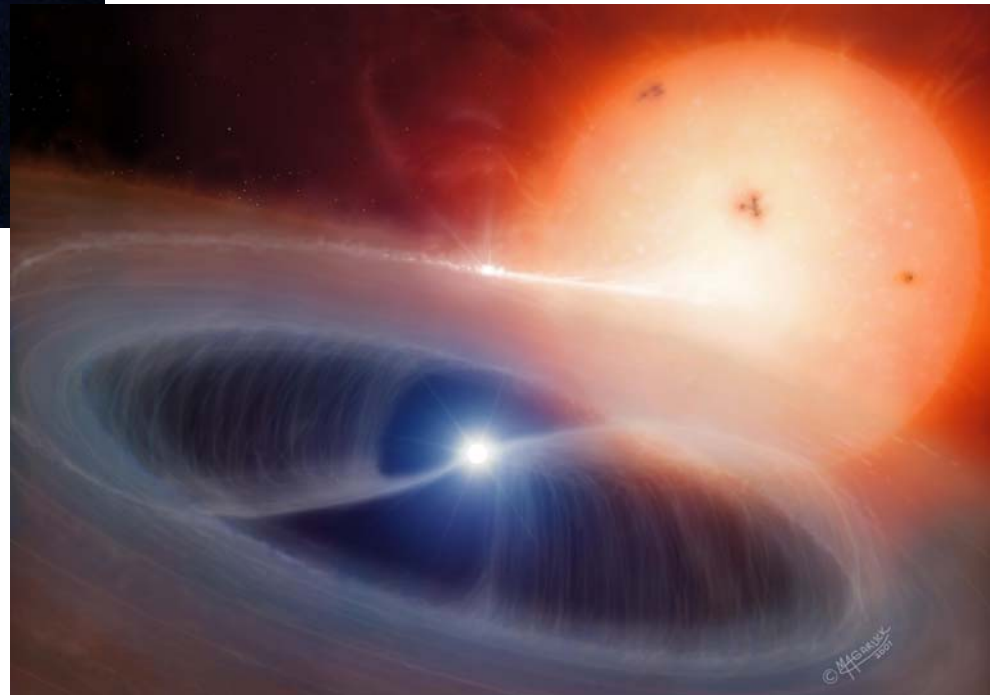
$$B \sim 10\text{-}200 \text{ MG}$$

Intermediate Polars

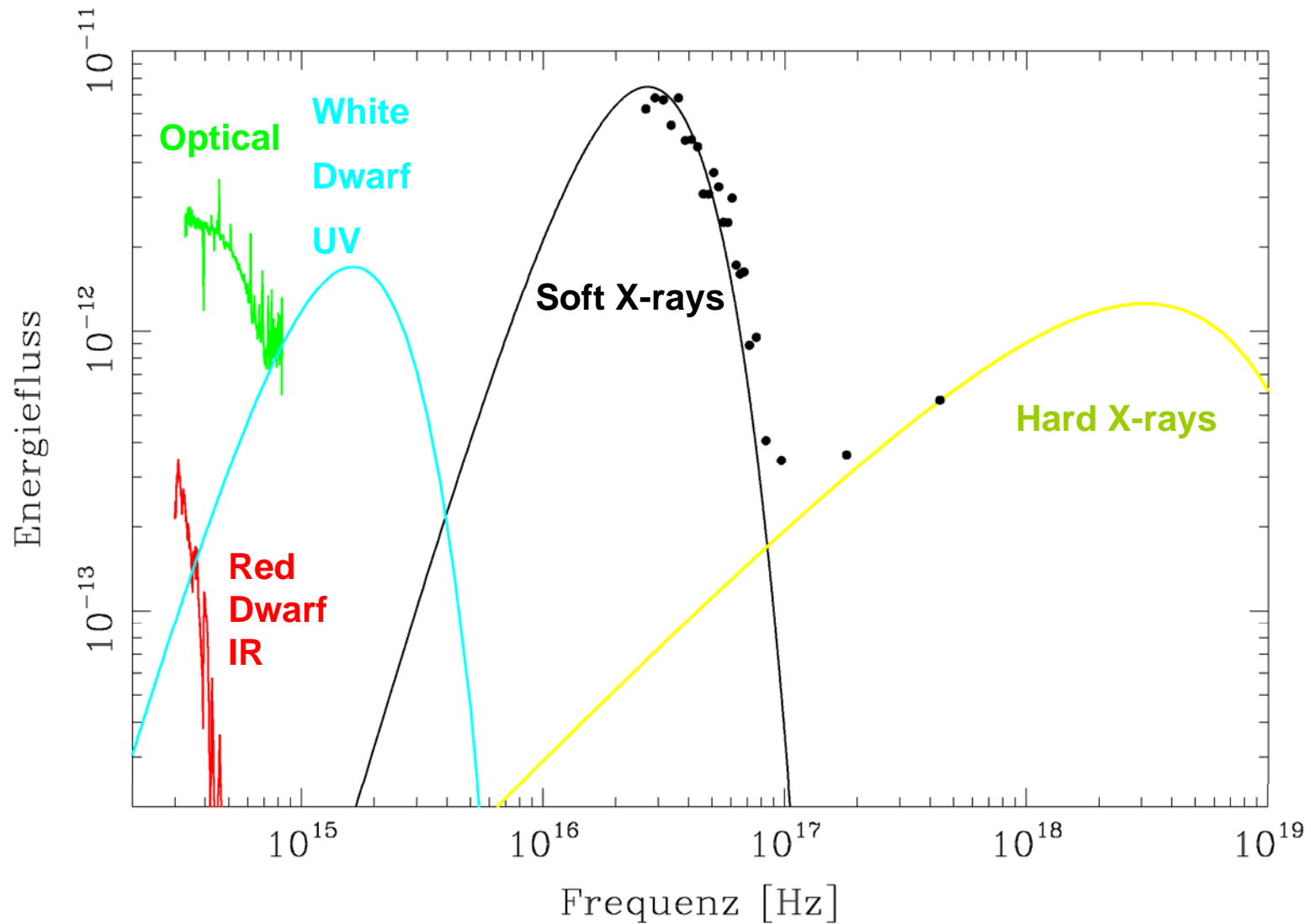
$$P_{\text{orb}} > P_{\text{spin}}$$

possible accretion disk

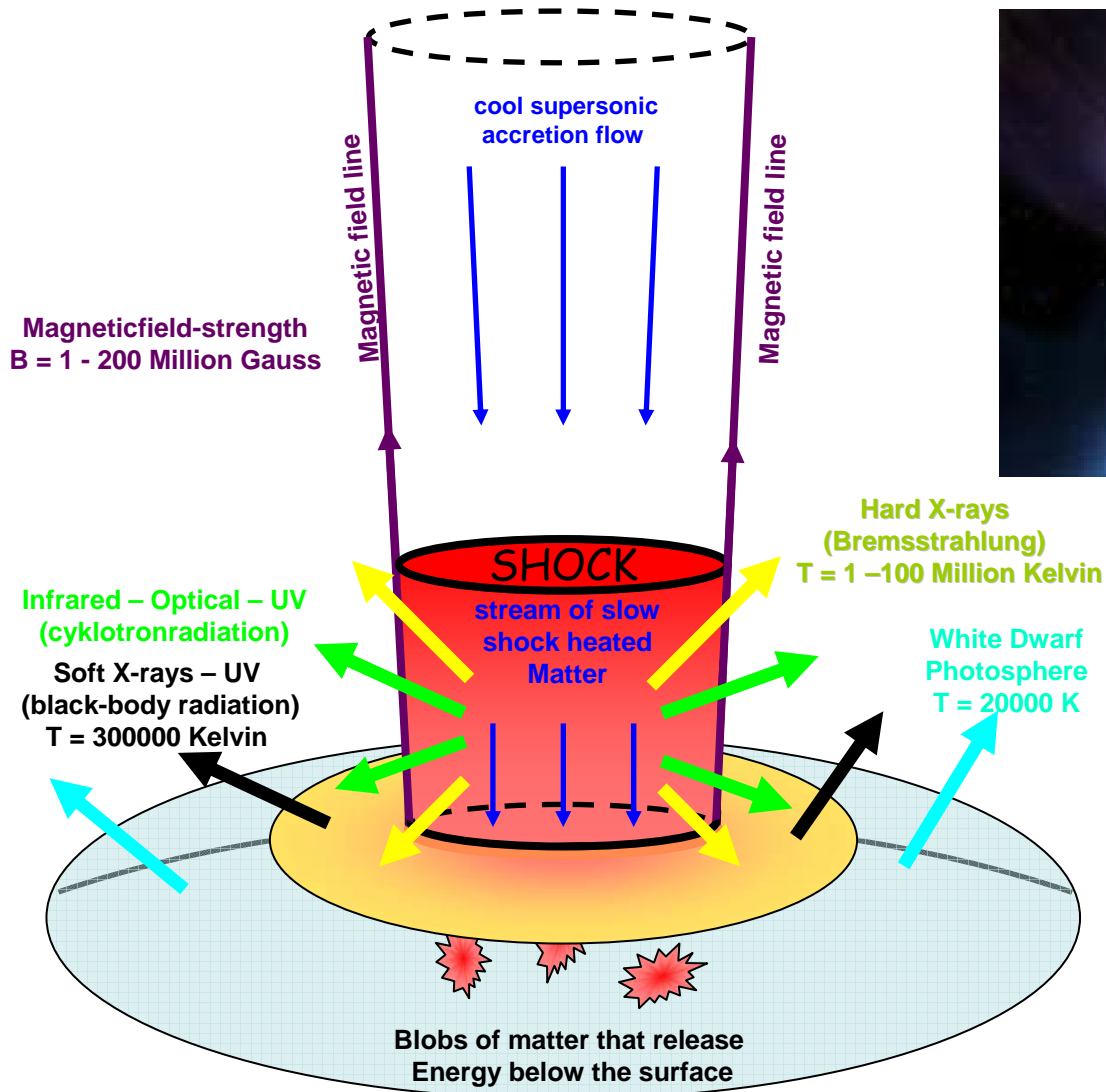
$$B \text{ upto } 20 \text{ MG}$$

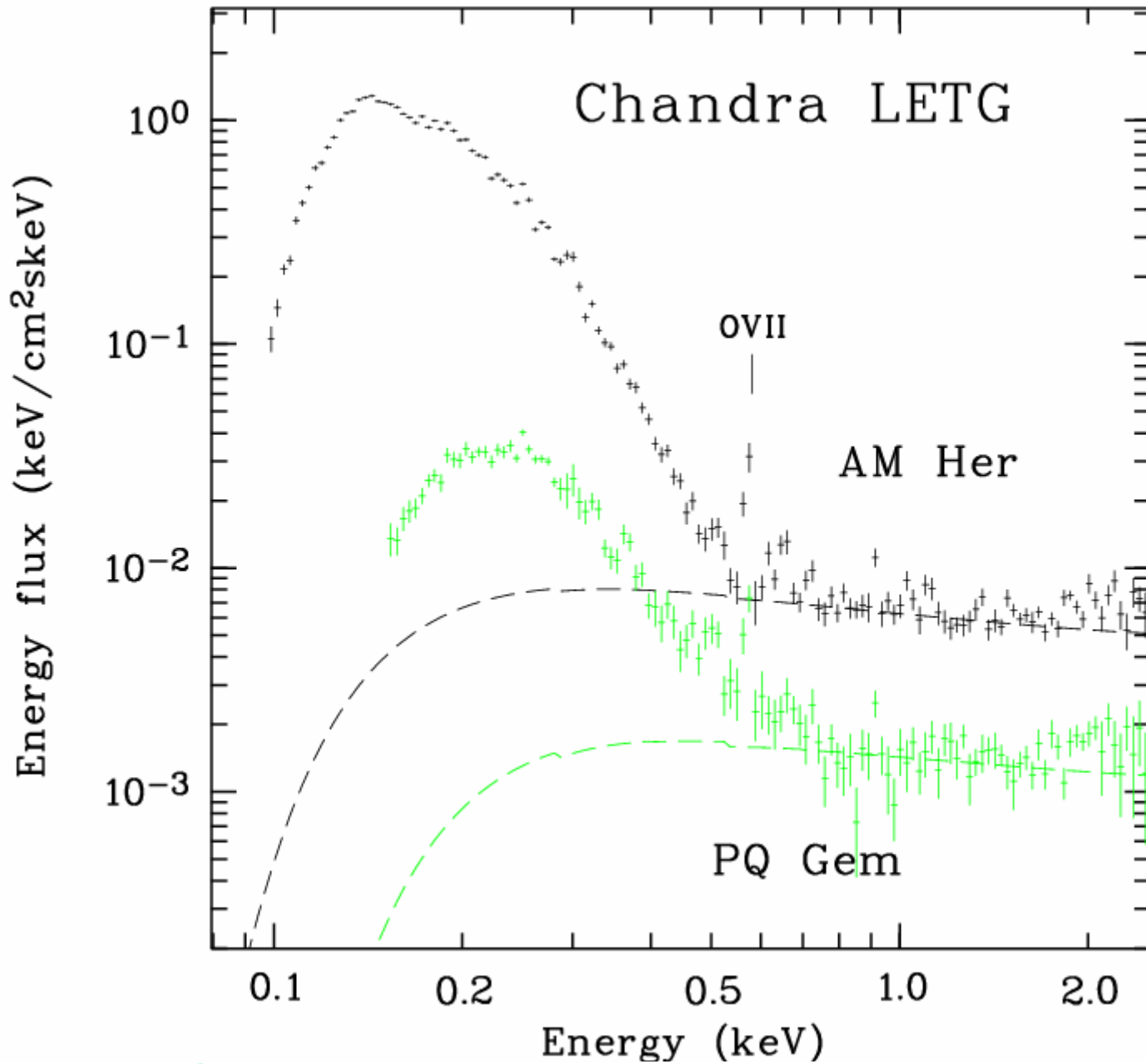


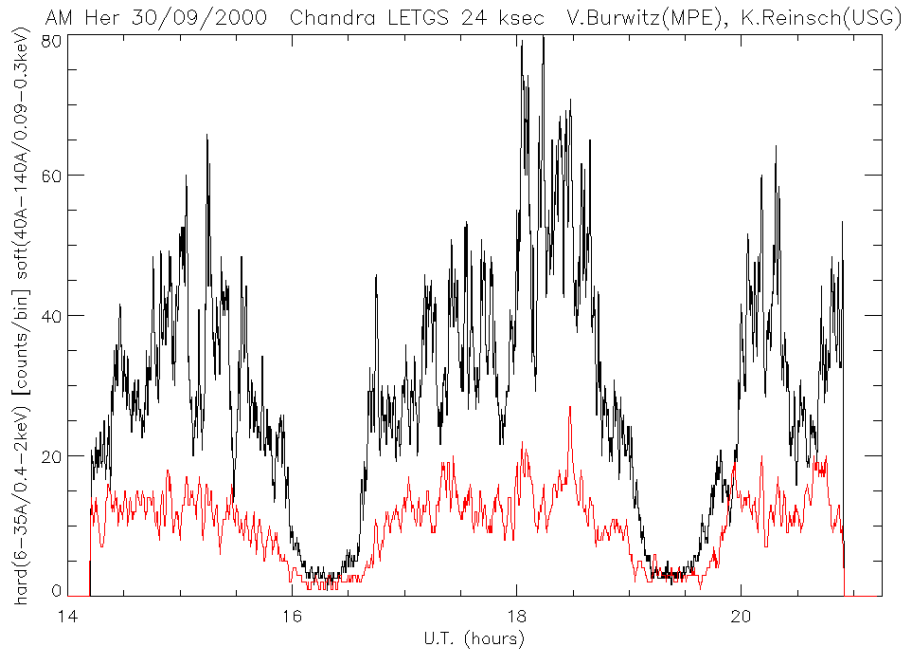
Overall spectrum of mCVs



Standard accretion scenario in mCVs







The Polar AM Herculis

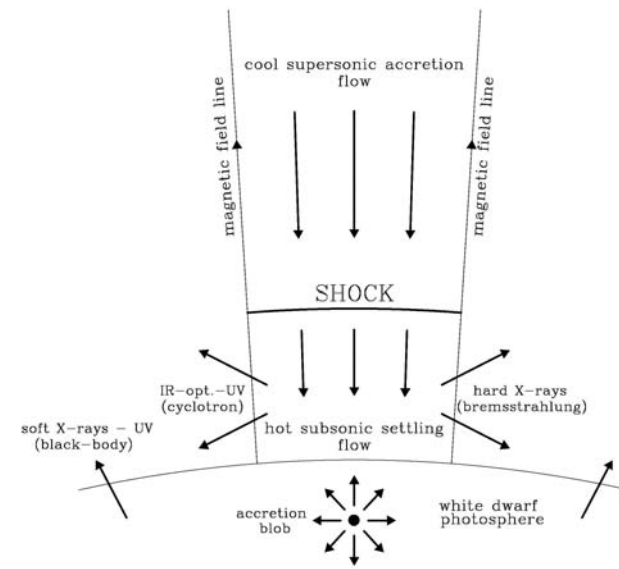
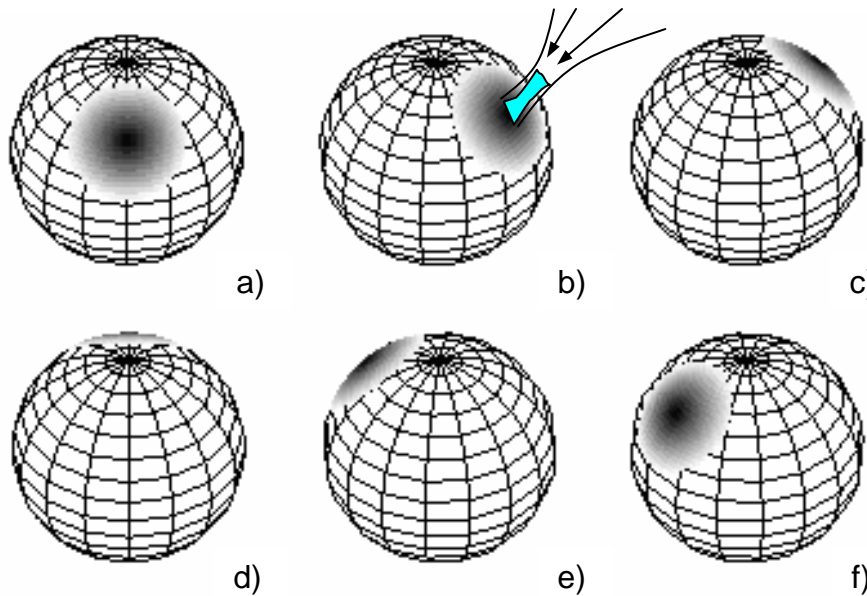
companion of type dM4

$P_{\text{orb}} = 186 \text{ min} = 3.1 \text{ hours}$

$d = 85 \pm 5 \text{ pc}$

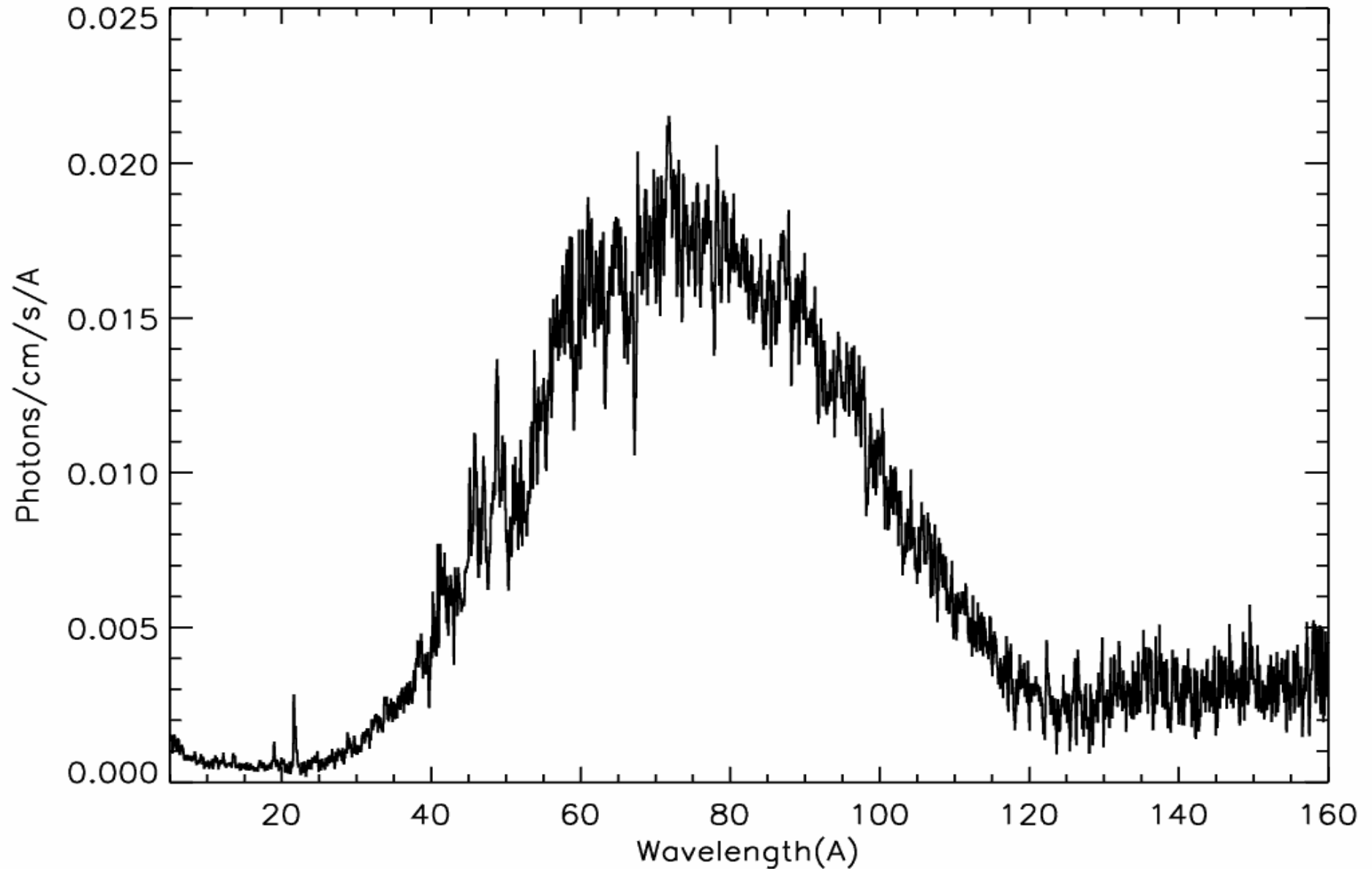
$B = 14.5 \text{ MG}$

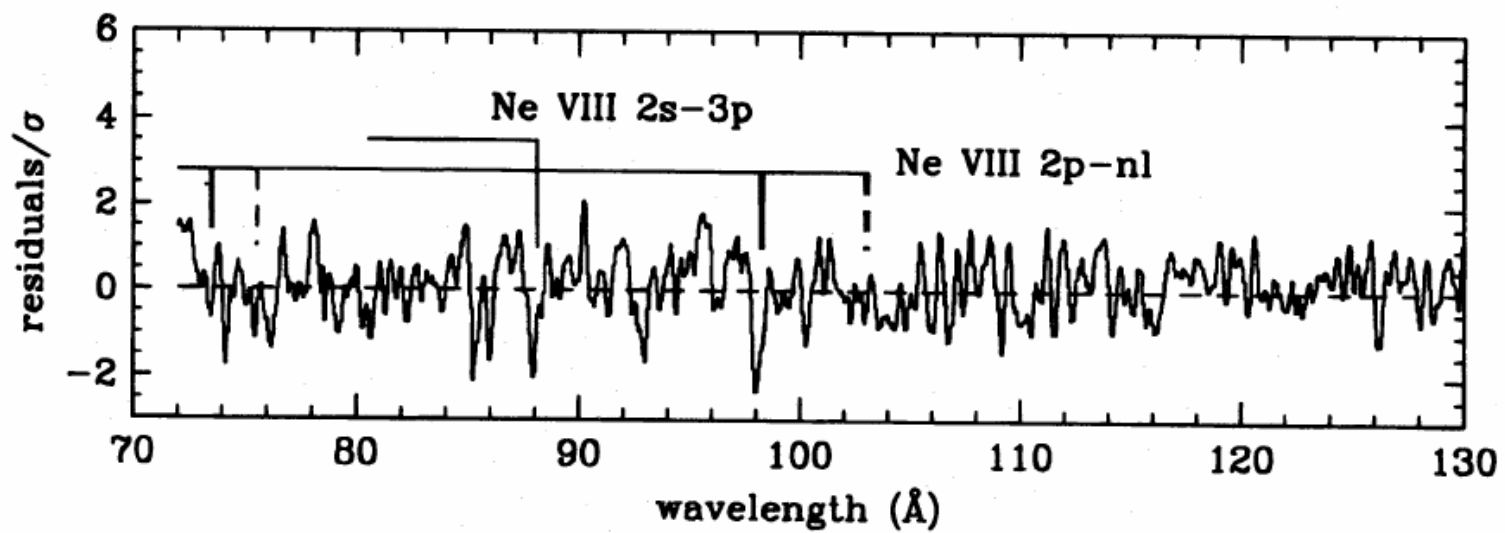
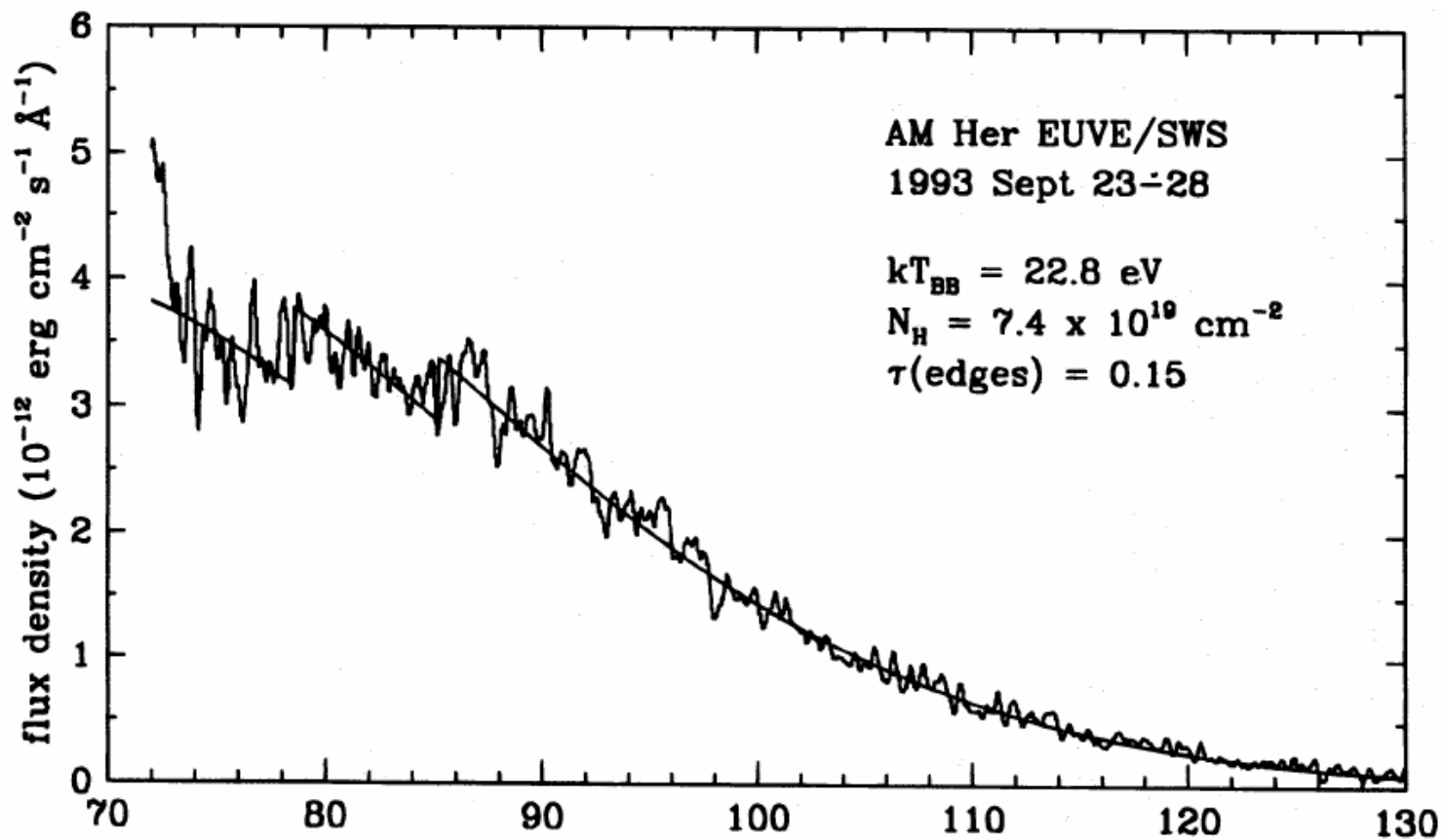
$T_{\text{wd}} = 24.000 \text{ K}$



AM Herculis: Spectrum (24 ksec)

AM Her Chandra LETGS





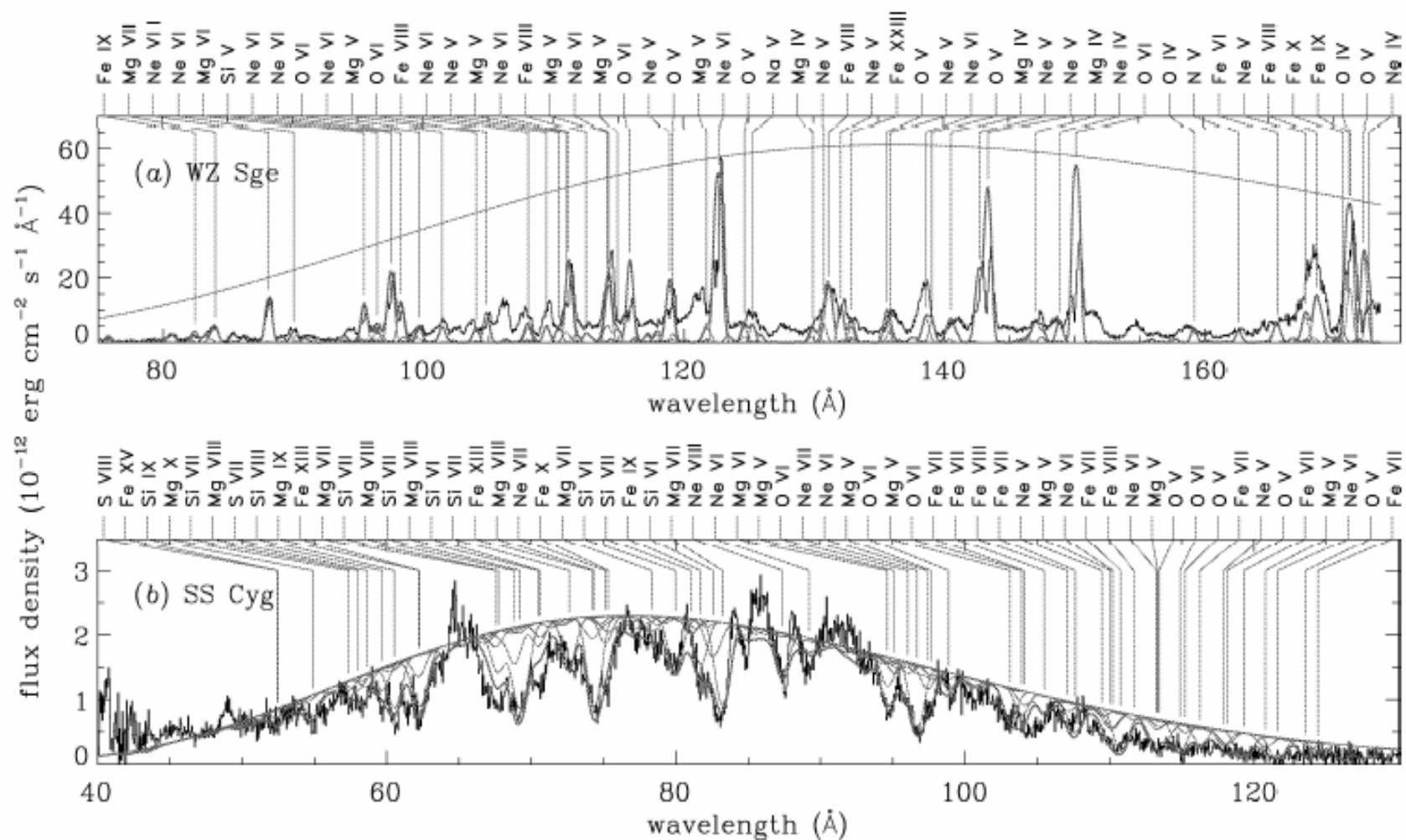
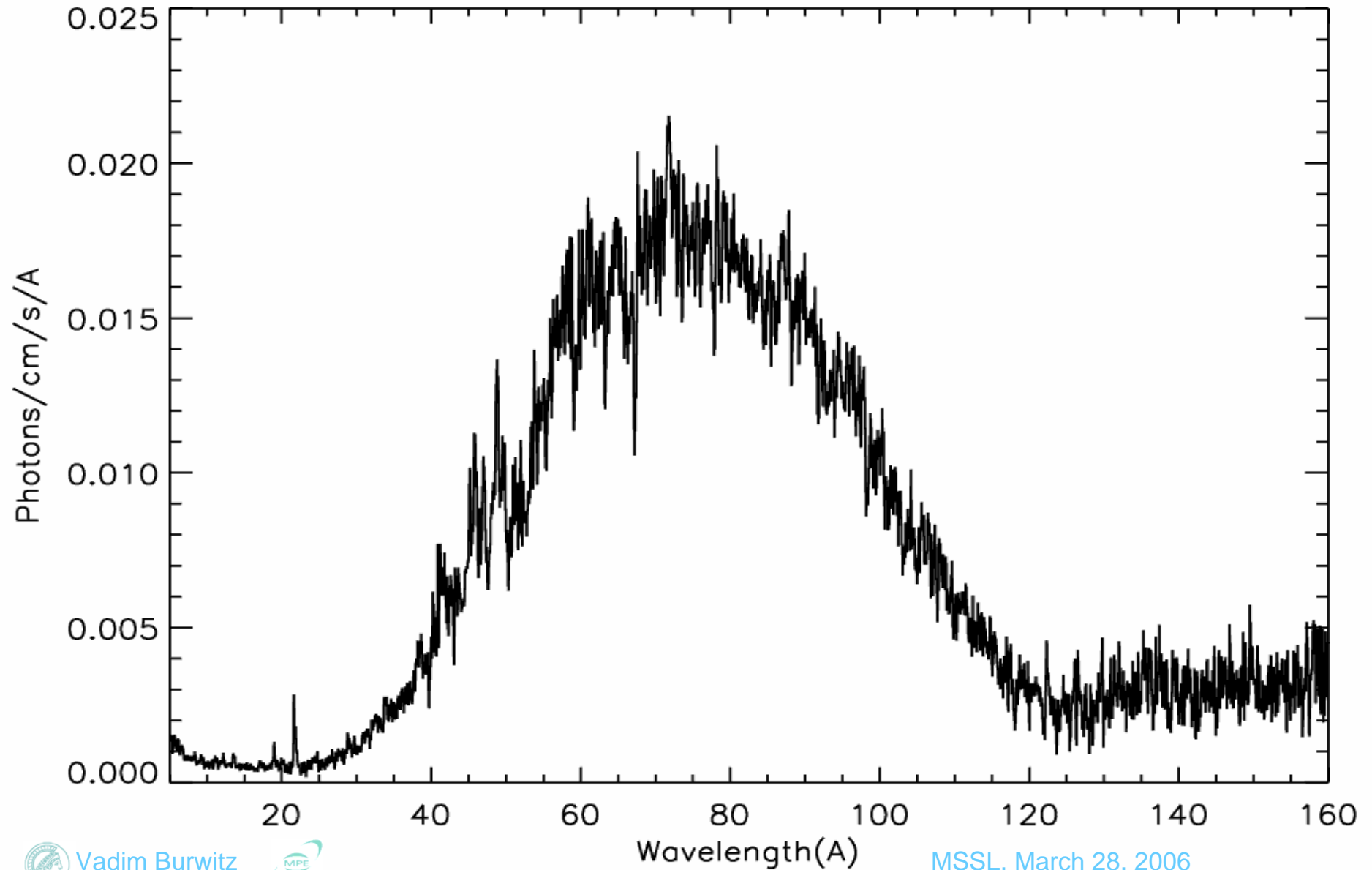
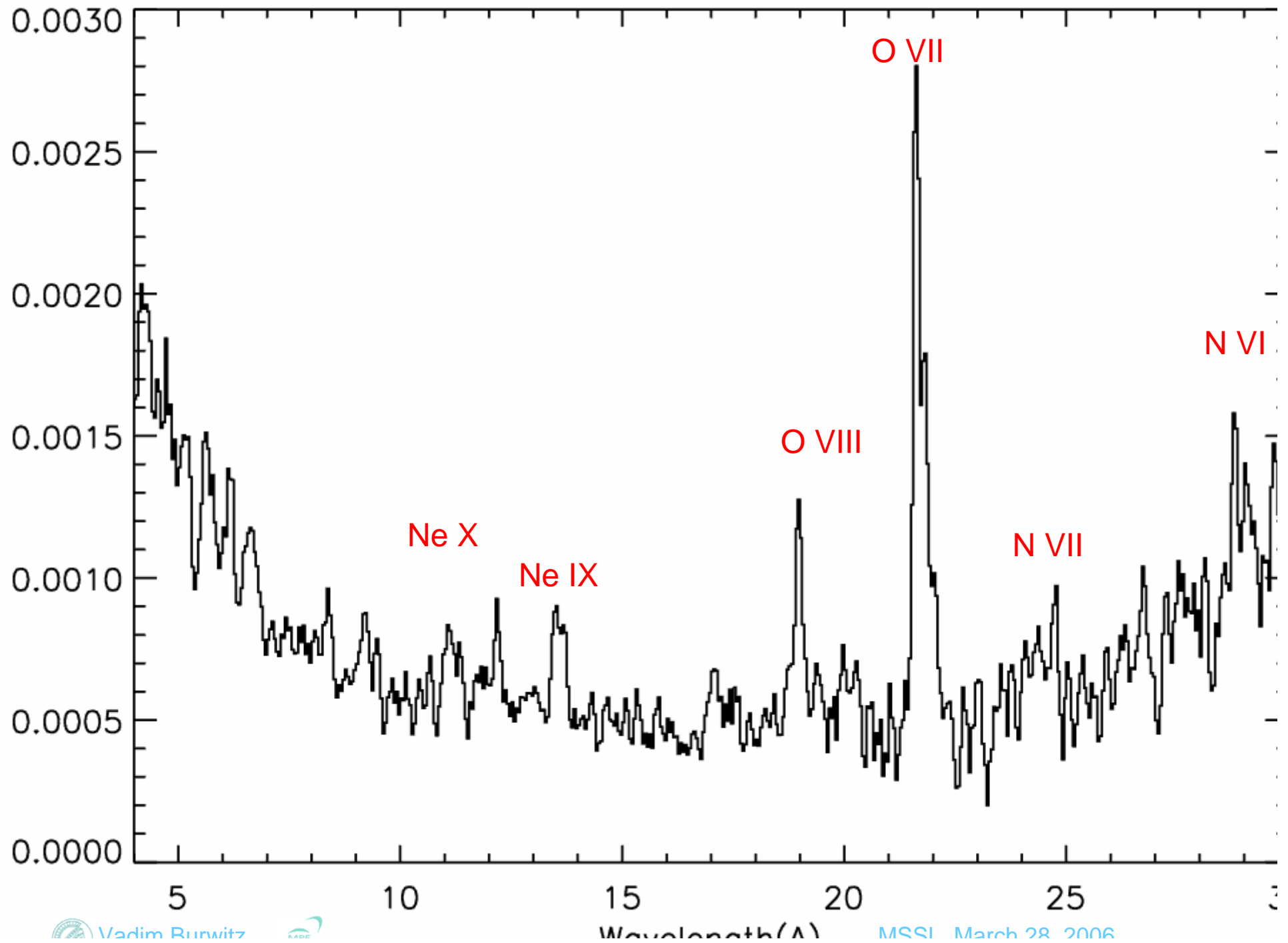


Fig. 3. *Chandra* LETG spectra of WZ Sge in superoutburst (*top panel*) and SS Cyg in outburst (*bottom panel*). The data are shown black and the model spectrum grey with the strongest lines indicated (from [54]).

AM Herculis: Spectrum (24 ksec)

AM Her Chandra LETGS

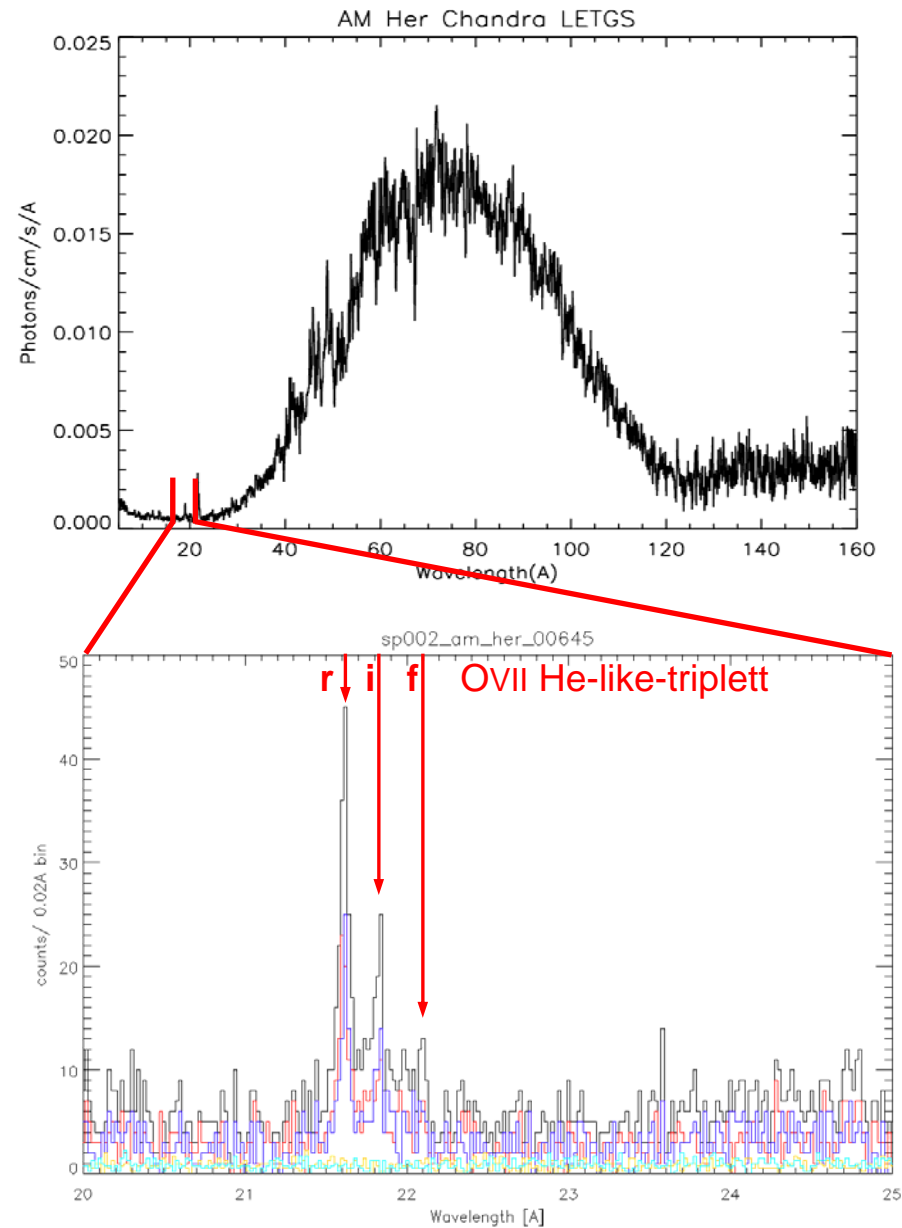
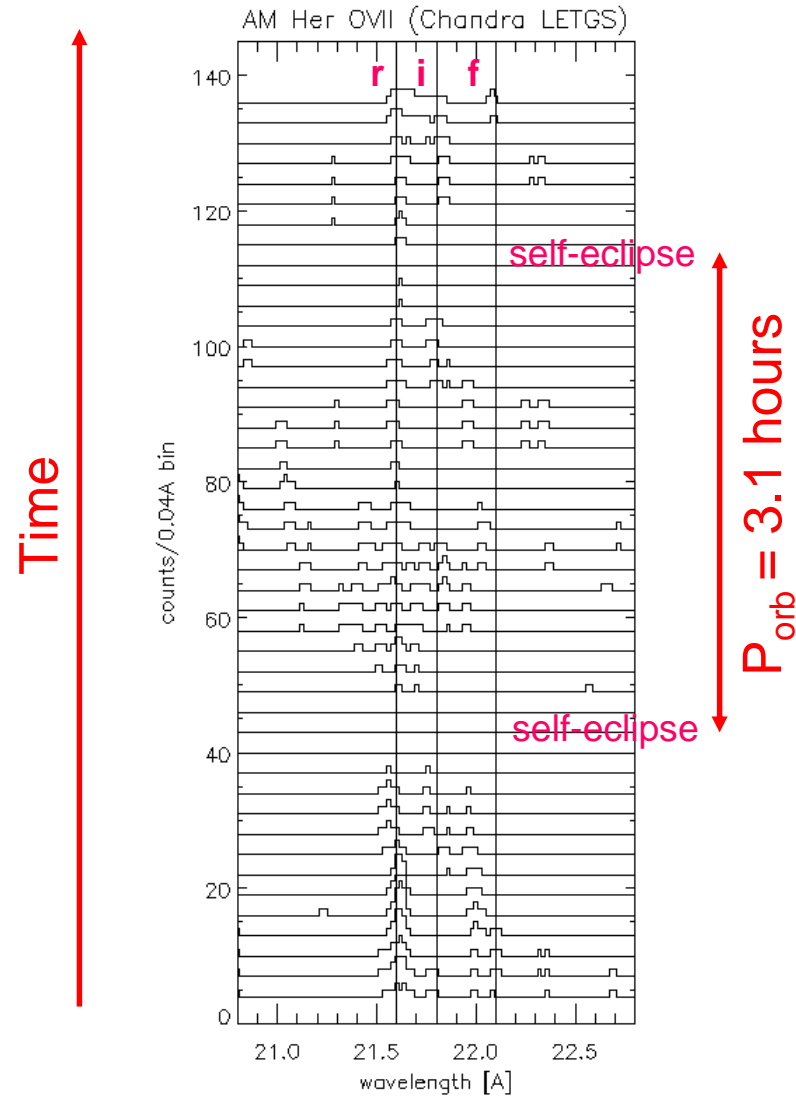




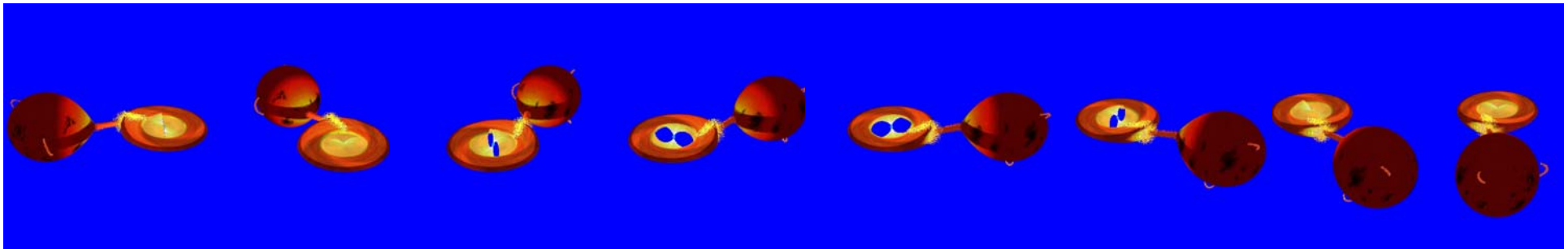
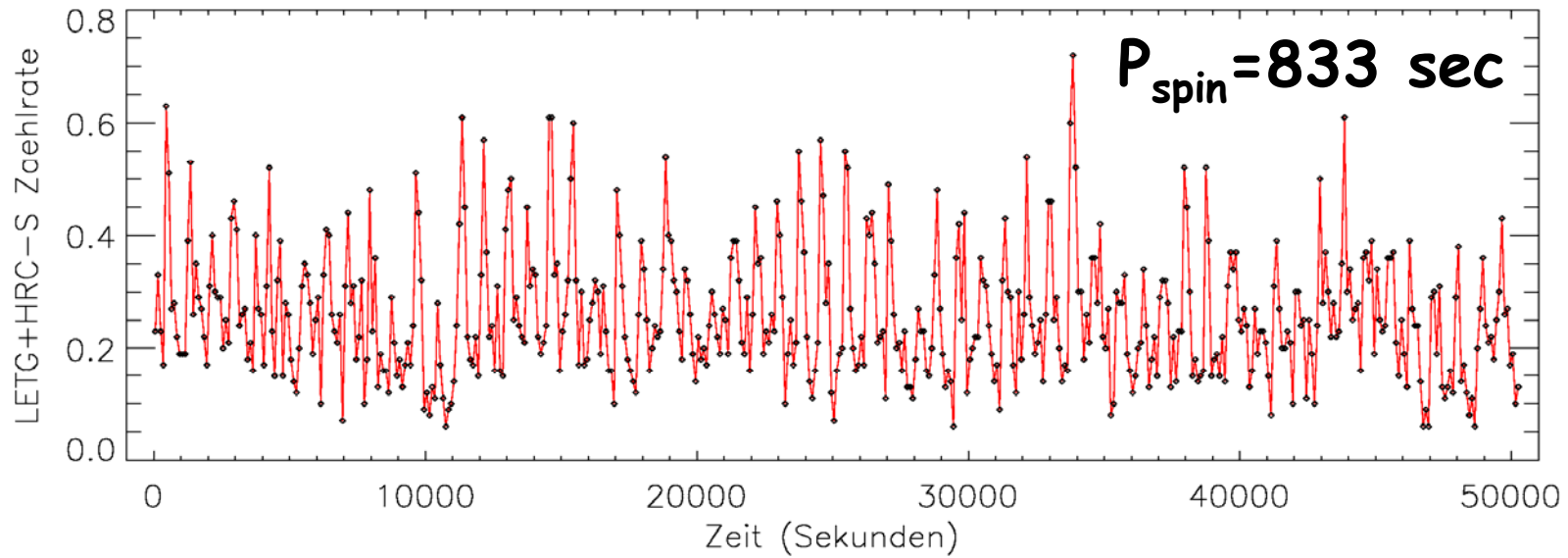
AM Herculis: Spectra

Chandra LETGS spectra (24 ksec)

Doppler Shift $\sim 0.05\text{\AA}$ @ 22\AA \Rightarrow $\sim 750\text{km/s}$

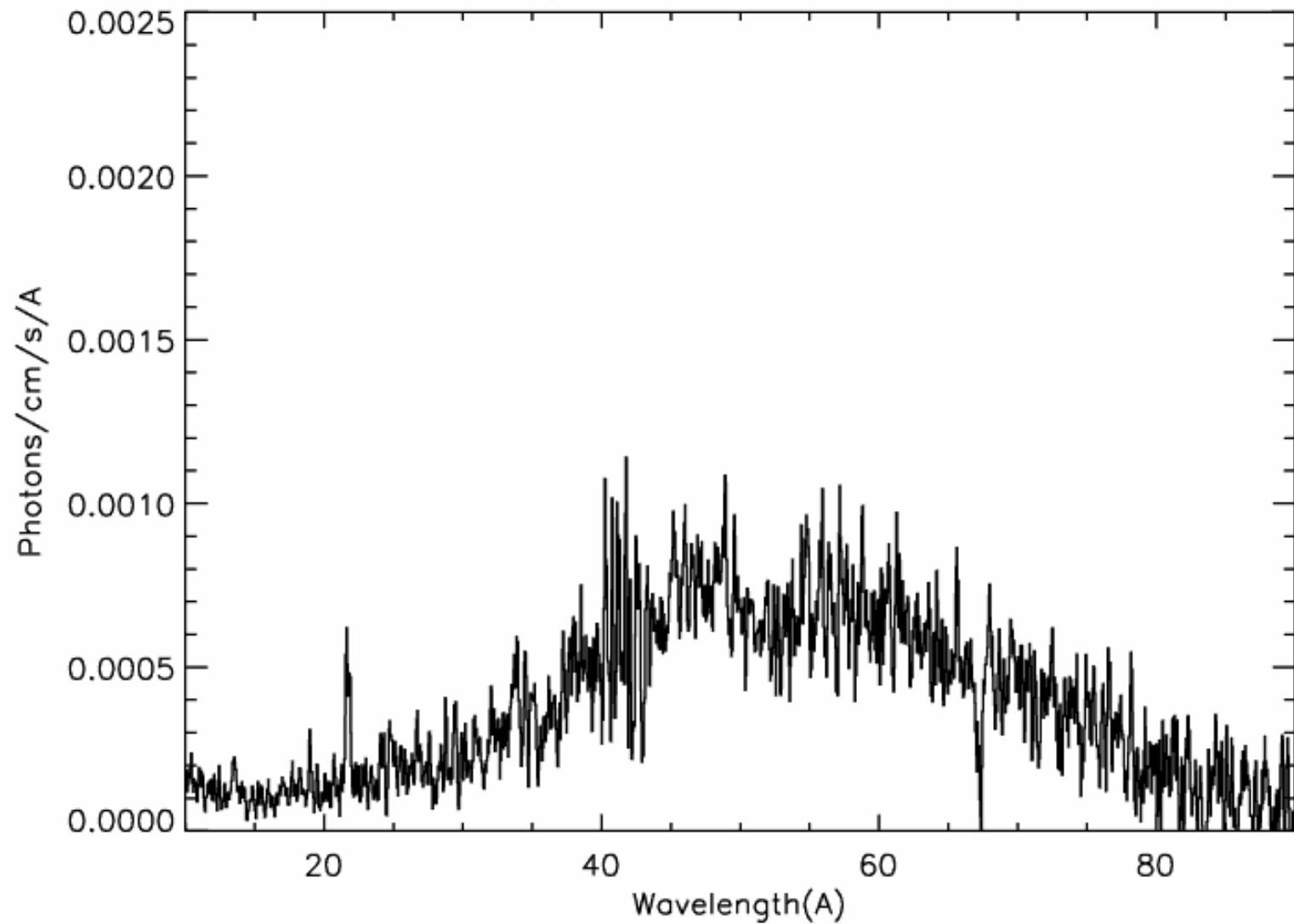


Chandra X-ray lightcurve of the intermediate polar PQ Gem

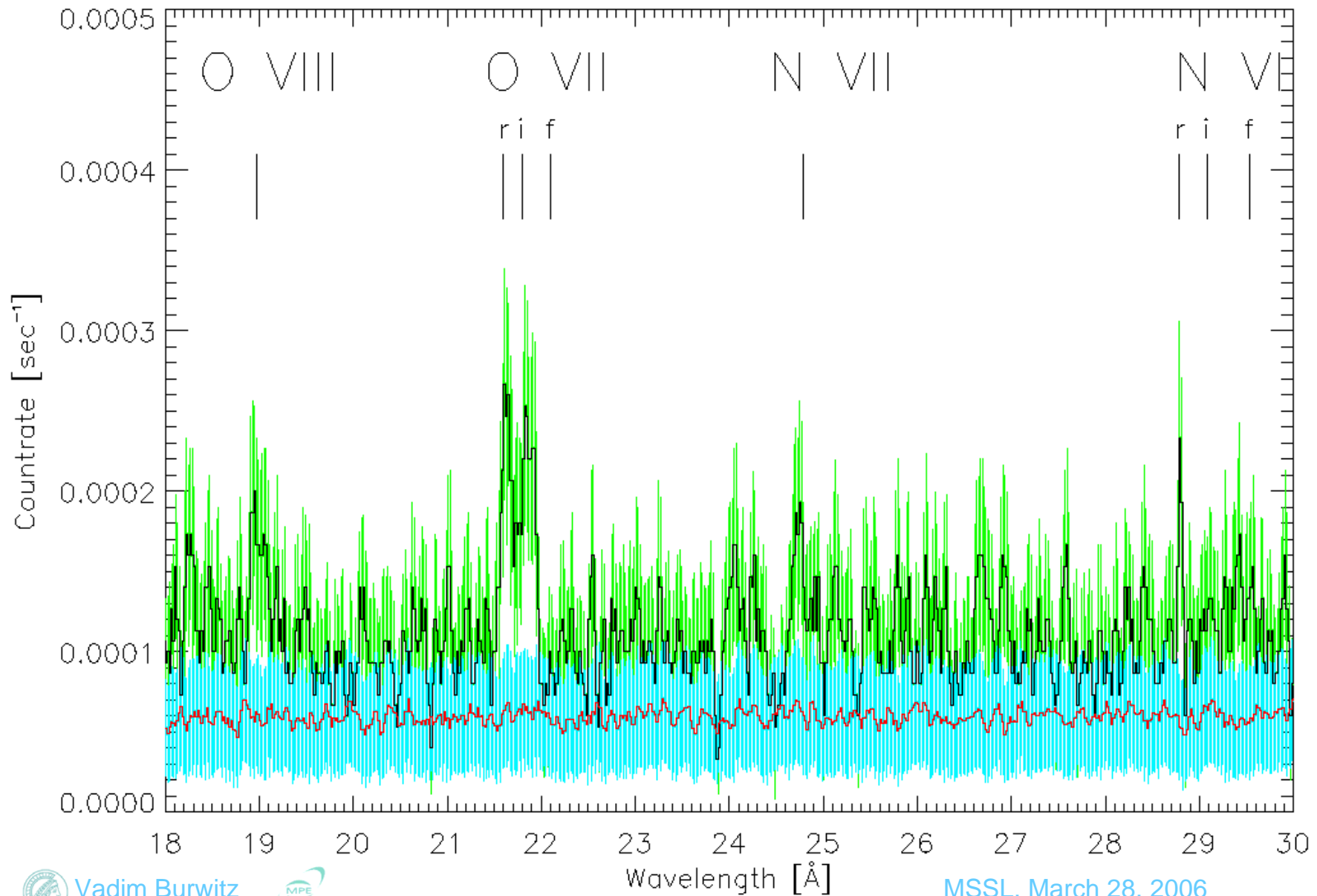


PQ Geminorum: Spectrum (50 ksec)

PQ Gem Chandra LETGS



PQ Gem: OVII and NVI He-Like tripletts



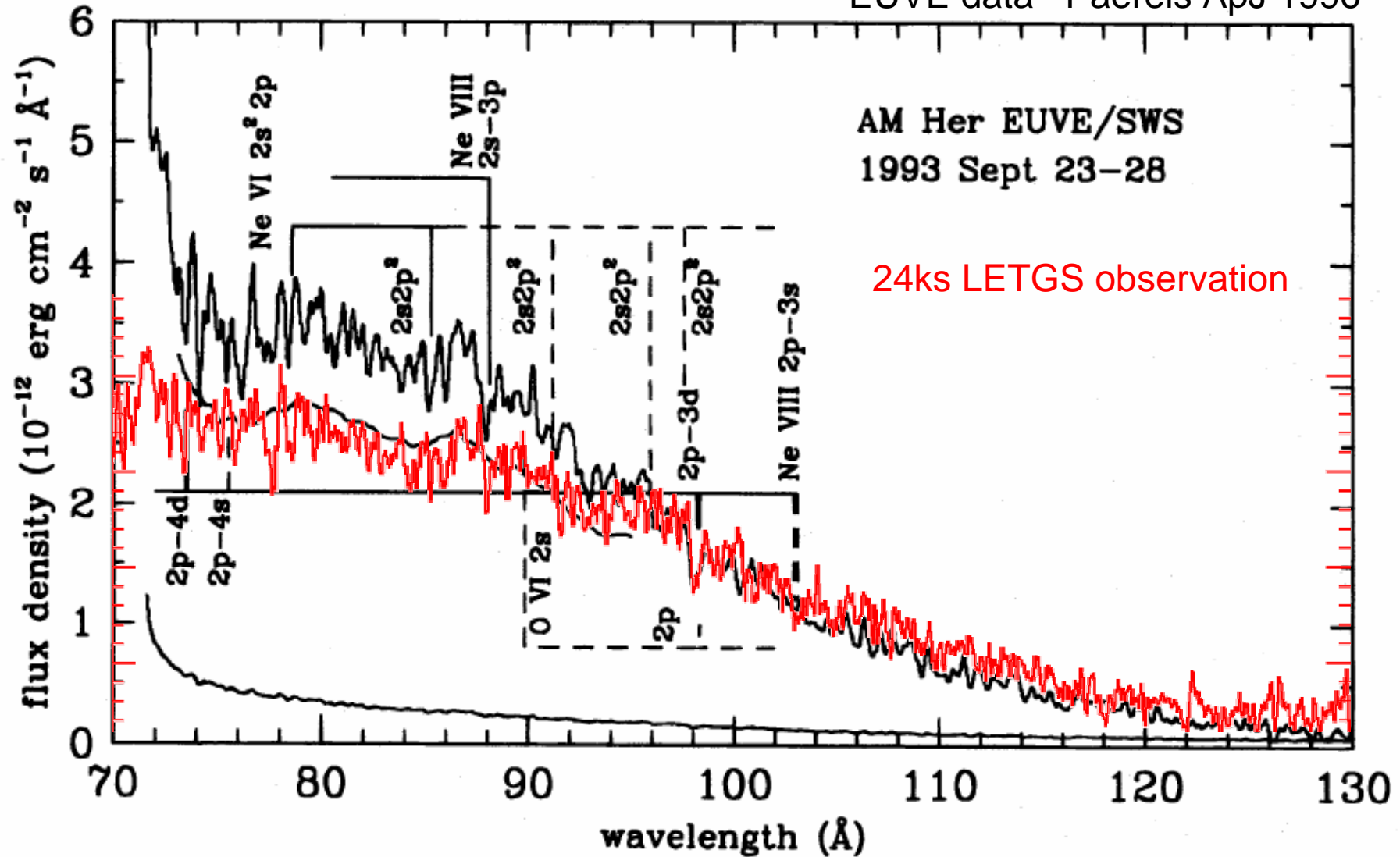


FIG. 1.—EUV spectrum of AM Her summed over all binary phases. Detector background has been subtracted; fluxes shortward of 73 \AA are too close to the detector edge to be reliable. The lower curve is an estimate of the uncertainty in the flux, based on counting statistics only. Spectral resolution is about $\sim 0.5 \text{ \AA}$. The positions of the Ne VI $2s^2 2p$ and $2s2p^2$ edges are indicated by solid lines; positions of edges from higher excited states (not seen) are marked by dashed lines, as are the positions of the O VI $2s$, $2p$ edges. Positively detected Ne VIII lines are indicated by solid lines. Also plotted is part of the spectrum smoothed over a 2.2 \AA range to emphasize the Ne VI edges (scaled by a factor 0.8 for clarity).

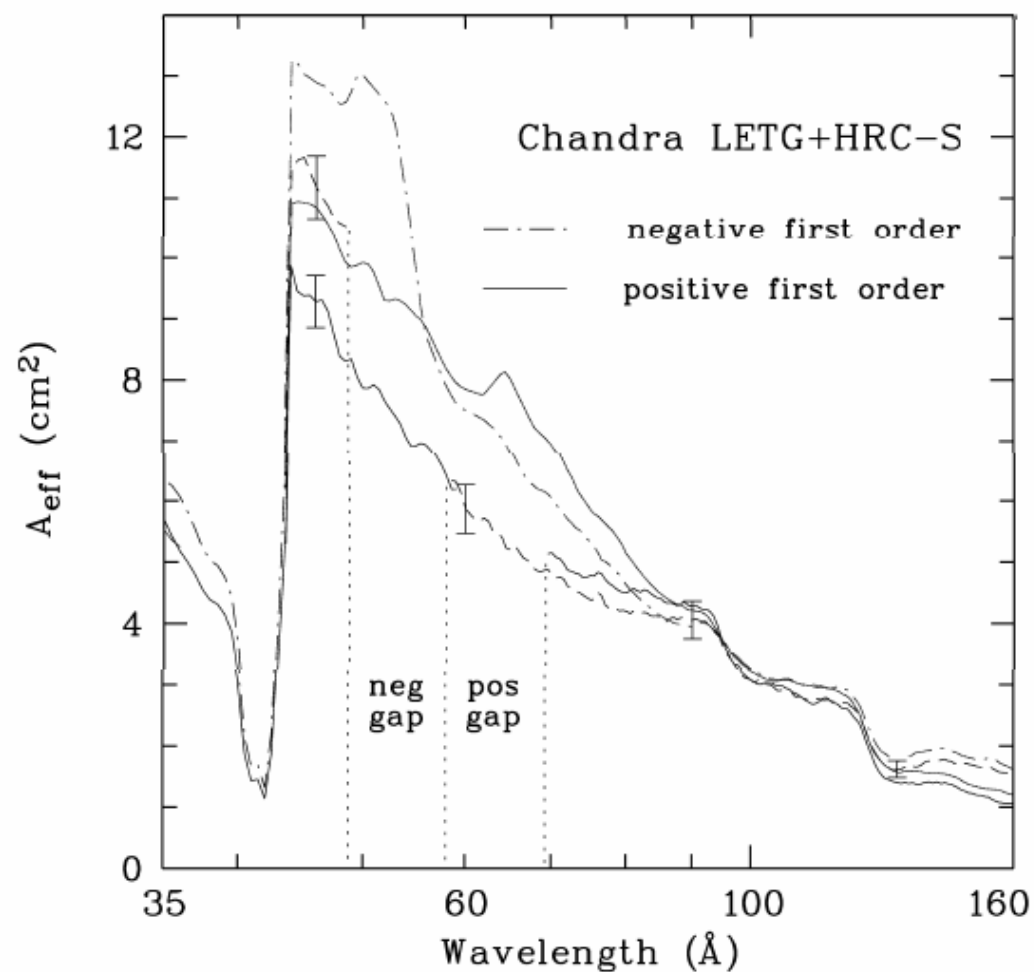
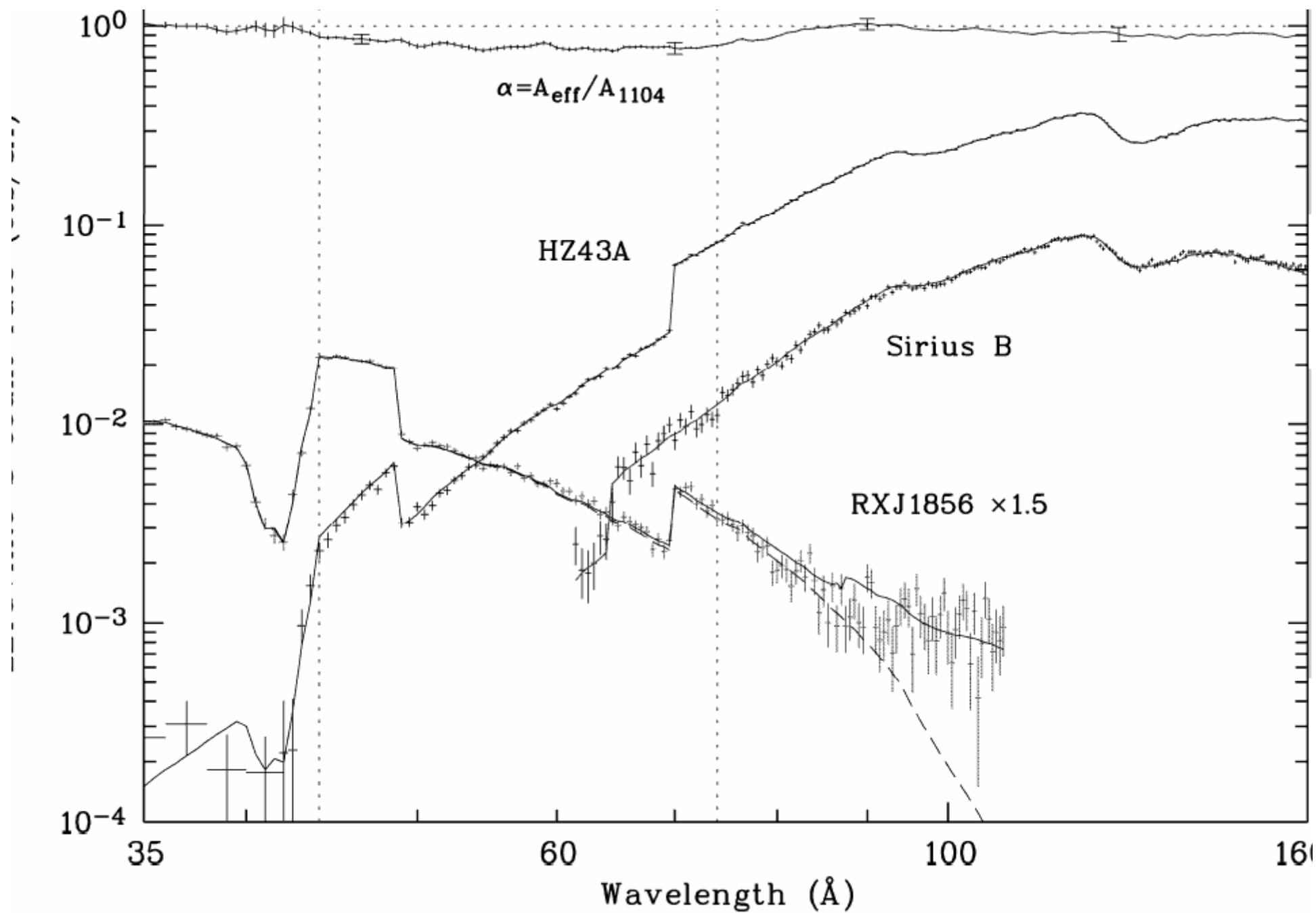


Fig. 5. Nominal effective areas of the *Chandra* LETG+HRC-S in the positive (solid curves) and negative (dot-dashed curves) dispersion directions of the November 2004 calibration data release (blue/grey curves) and the corresponding empirically adjusted effective areas (black curves) created with $\log g = 7.90$ for HZ43 A. They correspond to the correction function $\alpha(\lambda)$ displayed in Fig. 4. The systematic errors of this adjustment are indicated at four wavelengths.



taneous fit of RXJ1856, HZ43 A, and Sirius B in the wavelength ranges marked by vertical dotted lines. The LETG spectra are shown as data points, the corresponding best fit models as solid curves, and the first order contributions as dashed curves.

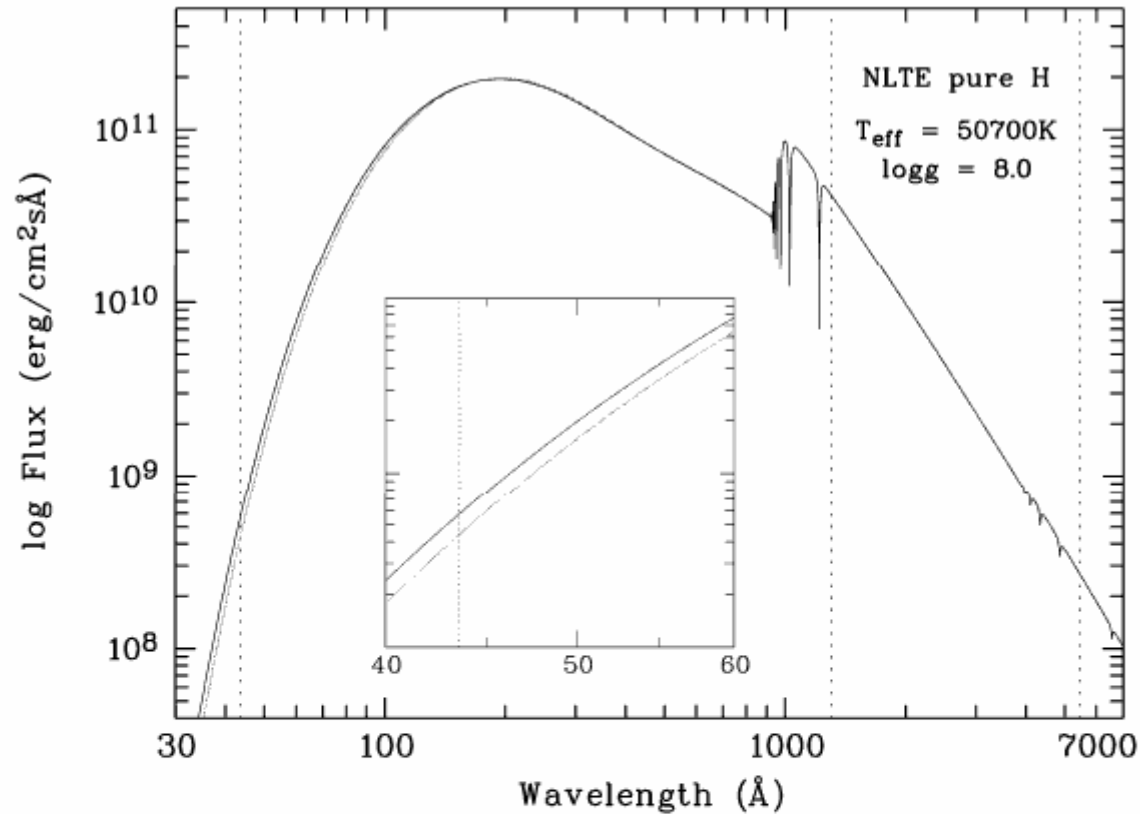


Fig. 1. NLTE pure hydrogen spectra for $T_{\text{eff}}=50700$ K and $\log g=8.0$, calculated with TMAP using two versions of the bound-free and free-free absorption coefficients, Seaton's approximation (green/grey curve) and the full Karszas & Latter (1961) description (black curve). Both models yield practically identical results at optical/ultraviolet wavelengths, but differ by a factor of 1.33 at 44\AA (vertical dotted line). The insert shows an expanded view. Two further dotted lines mark $\lambda = 1300\text{\AA}$ and $\lambda = 5450\text{\AA}$ (see text).